Magnetic Resonance Imaging

5

Michele Anzidei, Fabrizio Boni, Vincenzo Noce, Daniele Guerrieri, Beatrice Sacconi and Carlo Catalano

Abstract

Magnetic Resonance (MR) plays a leading role in pain imaging, offering optimal anatomic imaging and contributing functional and chemical studies of Central and Peripheral Nervous System. These tools have increased the comprehension of different chronic painful syndromes and the evaluation of treatment response to pharmacological or other therapeutic interventions. Furthermore, several neuro-MRI techniques, including functional magnetic resonance imaging (fMRI), MR spectroscopy (MRS) and diffusion-weighted imaging (DWI), have been demonstrated to depict nervous system pathologies associated with pain. Also, body MRI may be useful to depict several causes and manifestations of pain, local or diffuse, acute or chronic, covering the entire spectrum of disorders, supporting a multidisciplinary diagnosis process. In this section, after a brief discussion of MR basics, the main imaging procedures and their application in assessing the main painful syndromes will be deeply explored, with support of pictorial essays for each technique.

Keywords

Pain · MRI · Brain · Spinal cord · Nerves · Functional imaging

1 Introduction

Pain is defined by IASP Task Force as 'an unpleasant sensory and emotional experience associated with actual or potential tissue damage, or described in terms of such damage' [1]. Although many mechanisms of pain are not completely comprehended, the fast progress of imaging techniques in the last decades has provided remarkable advances in the understanding of painful conditions and their key mechanism [2]. Magnetic Resonance (MR) plays a leading role in pain imaging, offering optimal anatomic imaging and contributing functional and chemical studies of Central and Peripheral Nervous System. These tools have increased the comprehension of different chronic painful syndromes

M. Anzidei (✉) · F. Boni · V. Noce · D. Guerrieri · B. Sacconi · C. Catalano
Department of Radiological Sciences, University La Sapienza, Rome, Italy
e-mail: michele.anzidei@gmail.com

L. Saba (ed.), *Neuroimaging of Pain*, DOI 10.1007/978-3-319-48046-6_5

and the evaluation of treatment response to pharmacological or other therapeutic interventions. Furthermore, several neuro-MRI techniques, including functional magnetic resonance imaging (fMRI), MR spectroscopy (MRS) and diffusion-weighted imaging (DWI), have been demonstrated to depict nervous system pathologies associated with pain.

Neuroimaging studies identified many cortical regions involved in the perception of pain [3]; all the authors agree that pain is a complex neurological entity involving several networks and areas, comprehensively defined as 'pain neuromatrix,' including lateral components (primary and secondary somatosensory areas, S1\S2) and medial components (affective–cognitive–evaluative involving areas, like the anterior parts of insula, anterior cingulate cortex, and prefrontal cortex) [4]. These areas have been identified by using a study design defined as 'stimulate and see what you get'; the initial studies used PET to evaluate involved cortical regions by using painful stimuli. fMRI has been subsequently employed by using blood oxygen level-dependent (BOLD) method, reporting similar results to those of the first PET studies [5]. Other study designs have been developed, including those exploring other factors correlating with painful experience, such as anticipation, placebo effect, empathy, and differences between individuals in the pain perception; another extensive series of studies evaluated the effects of pharmacological and non-pharmacological therapies on pain, such as opioids, acupuncture, spinal cord stimulation, meditation, and hypnosis [6]. The list of pain conditions which can be evaluated by neuroimaging is large, including patients with chronic regional pain syndromes, chronic back pain, migraine, epilepsy, fibromyalgia, and chronic fatigue syndrome among others; the list of the available imaging techniques is also vast, including the already mentioned PET, SPECT, fMRI, MRS, DWI as well as diffusion tensor imaging (DTI) and pharmacological MRI (phMRI). The expectation for the next future would be to improve the capability of these imaging techniques in identifying the specific pain mechanisms in order to represent diagnostic tools for the individual patient evaluation, suggesting potential solutions for the single patient care.

Body MRI may be useful to depict several causes and manifestations of pain, local or diffuse, acute or chronic, covering the entire spectrum of disorders, supporting a multidisciplinary diagnosis process. For instance, wrist and hand MR imaging may play an important role in early diagnosis of rheumatoid arthritis and in developing the differential diagnosis for recent-onset arthritis [7].

In this section, after a brief discussion of MR basics, the main imaging procedures and their application in assessing the main painful syndromes will be deeply explored, with support of pictorial essays for each technique.

2 Magnetic Resonance Imaging

2.1 General Physical Principles

MRI takes advantage of the ubiquitous presence of hydrogen atoms or protons (H+) embedded in the water molecules and their magnetic dipoles in order to produce electrical signals by switching on and off external magnetic fields [8]. The entire process requires a magnet providing a constant magnetic field (B_0), a gradient system providing orthogonal fields for spatial localization of signals and a radiofrequency (RF) system with transmitter coils providing additional fields for spin excitation and receiver coils receiving MR signals over the imaging volume. When a volume is put inside a field B_0, all the H+ are aligned; by adding a set of RF and gradients, a selected slice of the volume is excited, the H+ are flipped out of their alignment and electric signals are transduced in the coils as the perturbed H + come back to their previous aligned state (relaxation) [9]. This is reached by using a specific MRI protocol including a pulse sequence, defining the characteristics of the RF pulse and a parameters set such as echo time (TE), repetition time (TR), matrix, field of view (FOV), and flip angles (FA). TE represents the time between RF excitation and first acquisition; TR is the time

interval between subsequent RF excitation per slice. By varying TR and TE, several MRI sequences can be performed, with different contrasts as per longitudinal magnetization recovery (T1) and transverse magnetization decay (T2); more in detail, long TR and TE lead to T2-weighted imaging, whereas short TR and TE to T1-weighted imaging. Each MR signal decodes for intensity, spatial and phase information; the different signal information is collected in the so-called k-space, which can be subsequently converted into a readable image by using a mathematical process (two-dimensional Fourier transform).

There are a large number of different sequences, which basically are classified into two families, spin echo sequences (SE) and gradient echo sequences (GE). The word 'pulse sequence' refers to a determinate series of radiofrequency (RF) waves or electromagnetic gradients, administrated in order to create MR images.

A typical SE sequence requires a 90° along with a slice selective gradient, and 180° RF pulse, whereas GE sequences are characterized by lack of the refocusing 180° RF pulse and a FA equal or smaller than 90°. Among specific sequences, it is worth to mention Echo-planar imaging (EPI) sequences, representing the base for several advanced techniques that will be covered in this chapter, such as DTI and fMRI. A dedicated MRI study of the brain can include, beyond conventional sequences, advanced imaging sequences, such as fMRI, MRS, ASL, DTI, with special reference to the individual clinical case.

All these MRI techniques will be more specifically described in the present section, both in terms of technical principles as well as in the present and potential clinical applications in several pain conditions.

2.2 Conventional MR Sequences

All conventional MR pulse sequences are derived by classical Spin Echo (SE) and Gradient Echo (GE). The basis of conventional MR imaging in painful syndromes is to depict anatomy, to detect pathologic variants or abnormalities and to emphasize specific morphological changes in the tissue structure (inflammation, fatty degeneration, fibrosis, etc.).

2.2.1 Spin Echo Sequences

As aforementioned, SE sequences are composed of a fundamental sequence of 90°–180° RF pulses (Fig. 1). Modifying TR and TE, it is possible to highlight specific characteristics for each tissue, obtaining so-called T1-weighted (T1-w) and T2-weighted (T2-w) images.

More specifically, short TR and short TE (less than 700 and 30 ms, respectively) heighten differences in T1 properties between tissues (T1-weighting), while T2 weighting require long TE and TR (greater than 2000 and 80 ms, respectively); avoiding T1 and T2 dependence by using a long TR with a short TE it is possible to obtain a proton density sequence. Because of their long acquisition time, these classical sequences are actually less used; advances in MR technology have enabled a reduction in acquisition time with the use of fast SE sequences. In a fast SE (FSE) or turbo SE sequence (TSE), a single 90° pulse is applied to flip the net magnetization vector, after which multiple 180° rephasing pulses are applied (Fig. 2).

The 180° echo pulses generate the so-called echo train, and the total number of 180° RF pulses and echoes is referred to as the echo train length. By using FSE and TSE techniques a dramatic reduction of acquisition time is guaranteed. Main use of TSE is to acquire T2-w images, although it can be applied even to produce T1-w images. This is due to the significant reduction in scan time that can be achieved for long TR scans when modest echo train lengths are used. Echo train lengths less than 10 are typically used for brain and spine imaging, but very long echo trains (100 or more) can be used in abdominal imaging to acquire T2-weighted images in less than one second. These classic sequences (SE or TSE) with different weighting (T1, T2 or PD), allow to depict several causes and manifestations of pain, local or diffuse, acute or chronic, covering the entire spectrum of disorders, often allowing to get the diagnosis

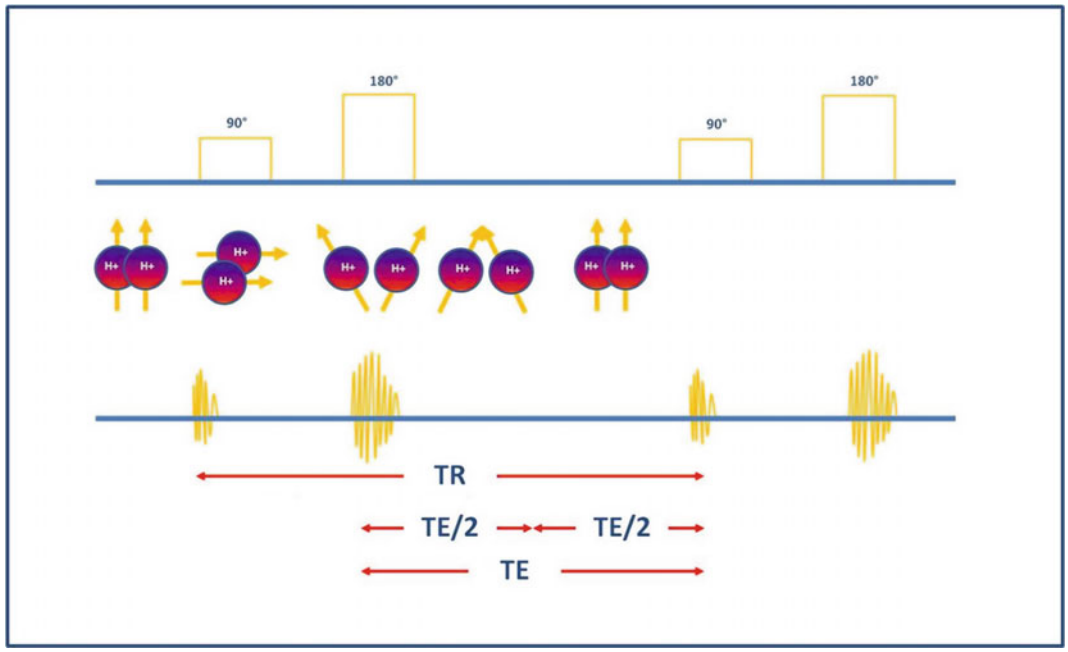

Fig. 1 Schematic representation of spin-echo sequences displaying radiofrequency pulses and consequent protons' excitement. *TR* Time of repetition. *TE* Time of echo

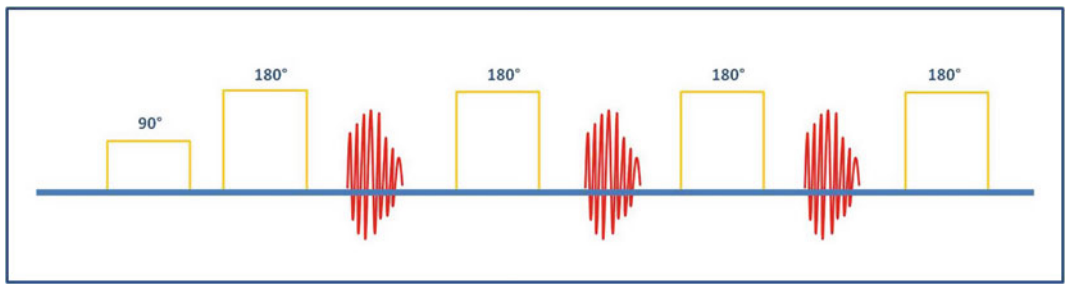

Fig. 2 Schematic representation of fast (or turbo) spin-echo sequences. The echo train is composed by a series of subsequent 180° pulses, permitting the acquisition of multiple lines of the volume for each TR, thus it allows an overall shortening of imaging time

without any other and more sophisticated processes (Figs. 3, 4, 5 and 6).

Use of paramagnetic contrast agent with T1-w sequences (TSE or GE) often offers more information, useful in diagnostic process (Figs. 7 and 8).

2.2.2 Gradient Echo Sequences

In order to reduce time of acquisition of standard SE, with a 180° pulse to refocus the protons, GE sequences (Fig. 9) employ gradient reversal pulses, in at least two directions, to generate echo signal.

The principal advantage of GRE technique is represented by its very short TR (that can be interpreted as faster time of acquisition). Table 1 resumes the main differences between classical SE and GRE sequences. GRE sequences may be classified coherent (refocused) or incoherent (spoiled) on the basis of the steady state phenomenon. This electromagnetic event is a

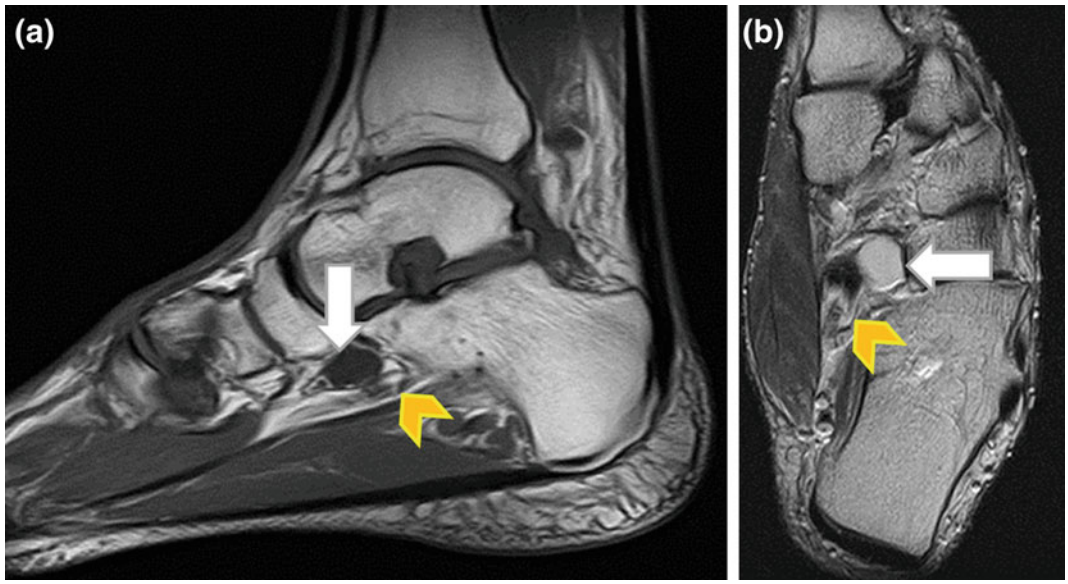

Fig. 3 Example of anatomic study by conventional T1-w and T2-w images. **a** Coronal T1-w of right ankle displaying fluid distension of synovial sheath, called ganglion cyst (*white arrow*), in tarsal tunnel. This abnormality causes tarsal tunnel syndrome, characterized by pain and paraesthesia in toes, sole, or heel, due to posterior neurovascular bundle (*yellow arrowhead*) compression. **b** Axial T2-w depicting a round fluid lesion (*white arrow*) in tarsal tunnel, conflicting with nervous–vascular structures

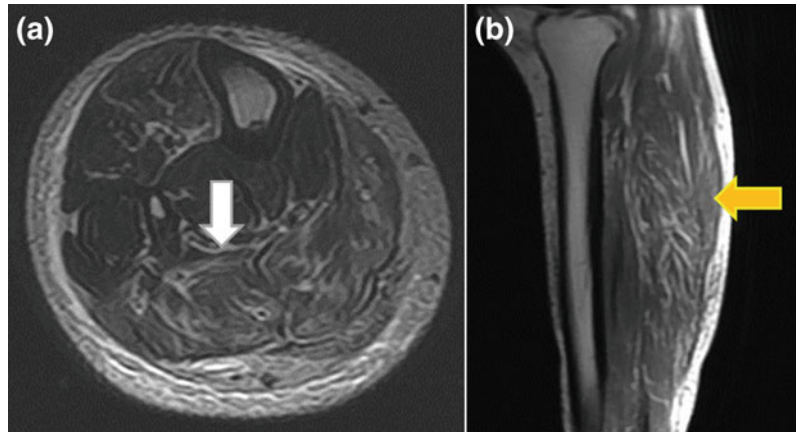

Fig. 4 Polymyositis. An autoimmune pathological process identifiable on MRI for a fatty infiltration around muscles, as well demonstrated on these T1-w (*white arrow*) and T2-w (*yellow arrow*)

consequence of extremely short TRs, usually shorter than T1 and T2 of the tissues imaged, causing a specific weighting called T2*, particularly sensitive and susceptible to magnetic field inhomogeneity. Coherent or partially refocused GRE sequences use a gradient to maintain the T2* and eventually produce T2-w images. The fundamental difference between partially refocused and fully refocused GRE sequences is that all the gradients in the latter are refocused. On the contrary, incoherent or spoiled GRE sequences utilize, after each echo, a specific RF

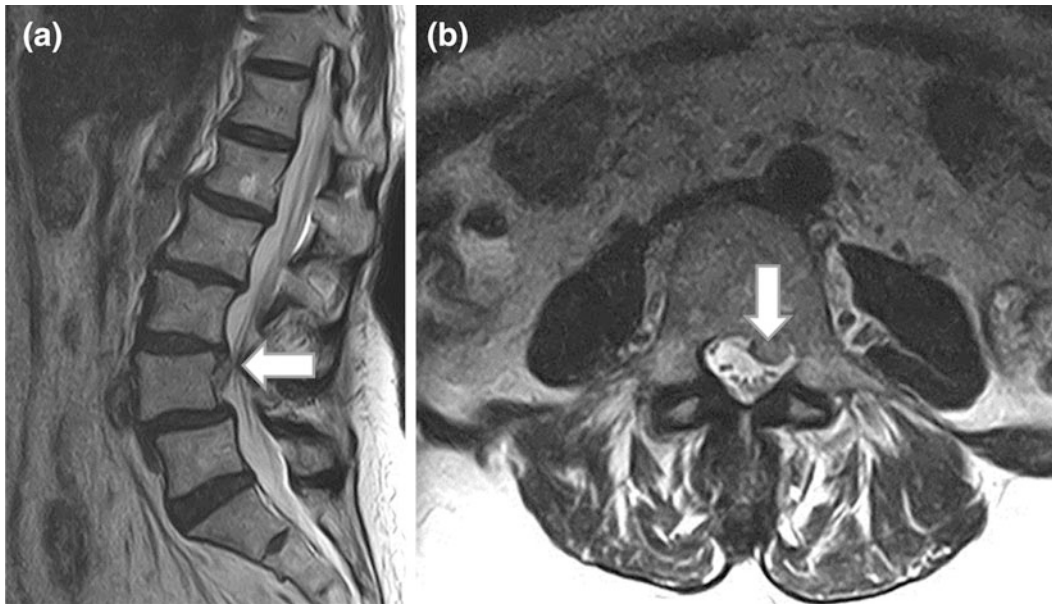

Fig. 5 Lumbar disc hernia. T2-w sagittal image (**a**) depicts a disc herniation (*white arrows*), with caudal migration, causing compression of left L4 nerve root at dural origin (**b**)

pulse or gradient, called spoiler, to null the T2* effect, thereby producing T1 or proton-density weighting. Partially refocused GRE images are mostly used in imaging of encephalic nerves and internal auditory canal structures (Fig. 10), while spoiled GRE sequences are widely employed in contrast-enhanced MRI.

Steady-state free precession (SSFP) represents a specific fully rephased GRE technique, with continuous repetition of short TRs (5 ms). SSFP guarantee the best temporal resolution among MR pulse sequences, high signal-to-noise ratio, but an extreme susceptibility to artifacts caused by magnetic field inhomogeneities. These sequences are employed in cardiovascular (Fig. 11) and gastroenteric imaging, due to high signal achieved from blood vessels and static fluids.

2.2.3 Fat and Fluid Signal Suppression

MRI permits the specific suppression or saturation of tissue signals; this tool is widely used to achieve a better characterization. Among the commonest structures that are suppressed in MRI there are fat tissue, cerebrospinal fluid, and silicon. Fat saturation is targeted to obtain diagnosis in case of lesions contacting adipocytes or intracytoplasmic fat, but it is advantageous even in order to enhance signal from other tissues, nulling the 'fat background' (e.g., edema imaging). At least three methods for fat nulling are routinely used in MRI. The commonest method for fat saturation is applying a frequency-selective saturation RF pulse or spoiler gradient to null fat signal, immediately subsequent to 90° initial pulse. This technology is fast, 'lipid specific' and because fat suppression is achieved by selective saturation pulse before normal acquisition, it can be used with any imaging sequences, particularly in contrast-enhanced MRI (Fig. 12); on the other hand, it may be hampered by artifacts due to magnetic field inhomogeneity and incomplete suppression.

The second method for fat signal nulling is Inversion Recovery (IR) imaging, obtained by application of an initial 180° to flip the net magnetization vector of fat tissue (STIR, Short Tau Inversion Recovery); the 90° pulse is the applied exactly at fat 'null interval' (140 ms) to suppress its signal (Fig. 13).

Fig. 6 Idiopathic spinal cord herniation. This condition is only encountered between T2 and T8 where the normal thoracic kyphosis leads to the thoracic cord being in close proximity to the ventral theca. The key feature is focal distortion and rotation of the cord with no CSF seen between it and the ventral theca (as well demonstrable on this T2-w image, *white arrow*)

STIR sequences are actually widely used in common MR protocols, from oncologic to musculoskeletal imaging, in order to detect solid lesions, as well as edema due to traumatic, functional or vascular injuries (Figs. 14 and 15). This technique is limited by long TR required, causing increase of acquisition duration.

The third method for fat suppression is the so-called 'Out-of-phase imaging'; using Spoiled GRE sequences this technique excites different precession rates between ^{1}H in fat (CH_2) and water (H_2O). When co-presence of CH_2 and H_2O happens in same volume, the signal is nulled. Note that this technique permits the suppression of 'microscopical fat' (steroids or triglycerides deposits), characteristically present in adenomatous cells and steatosis hepatocytes.

Suppression of signal applied to Cerebrospinal Fluid gains dramatic significance in neuroimaging; this technique is based on inversion-recovery SE sequences referred as FLuid-Attenunated Inversion Recovery (FLAIR). Nulling CSF permits detection of lesions otherwise not distinguishable, specifically if localized nearby sulci or ventricles, and edema in central nervous system, a signal of tissue damage from vascular cause or compression from a growing mass.

2.2.4 Proton Density Imaging

Setting a pulse sequence with long TR (2000–5000 ms) and short TE (10–20), differences between T1 and T2 relaxation times for different tissues will be minimized, while stronger signals

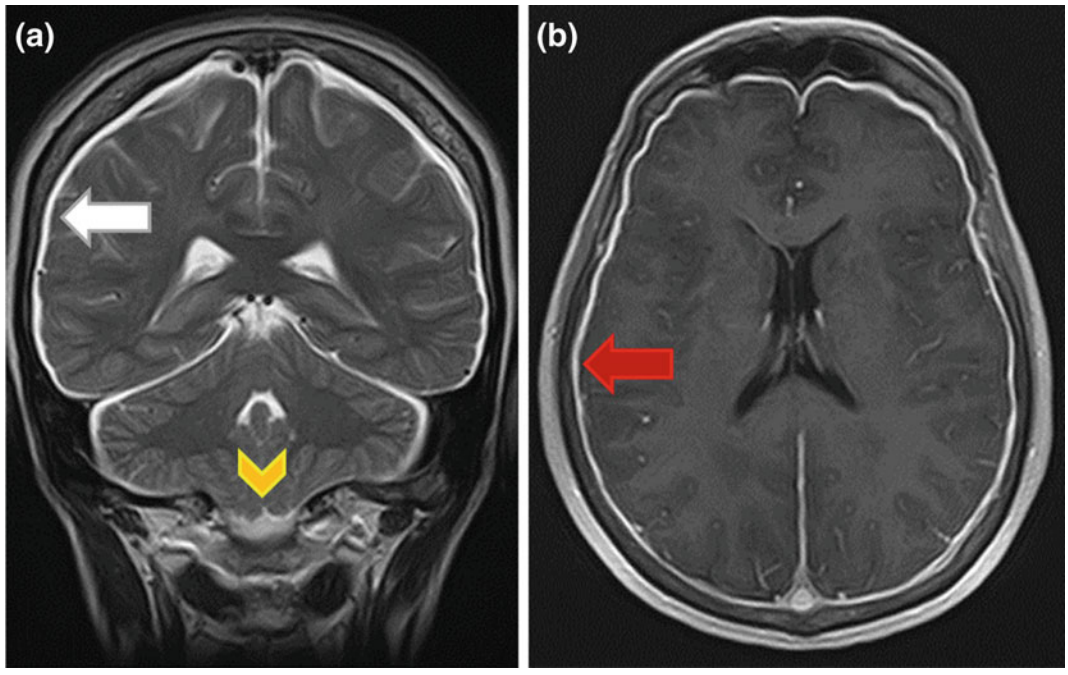

Fig. 7 Spontaneous intracranial hypotension. On the *left* (**a**, Flair) evidence of subdural effusion (*white arrow*) and cerebellar tonsillar ectopia (*yellow arrowhead*); on the *right* (**b**, T1-w post-Gd), diffuse pachymeningeal enhancement (*red arrow*)

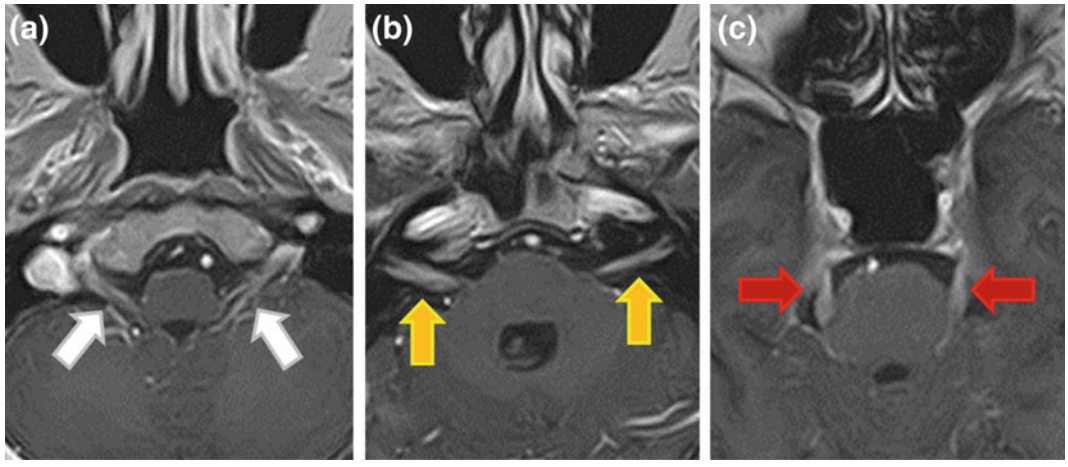

Fig. 8 Carcinomatous meningitis. On **a**, **b** and **c** images, T1-w post-Gd sequences showing significant enhancement of nerve sheaths in patient suffering from lung cancer (*white arrows* XI cranial nerves; *yellow arrows* VIII cranial nerves; *red arrows* V cranial nerves), indicating spread of malignant cells

are produced by structures with high density of hydrogen protons. This pulse sequence design is called proton density (PD) weighting. PD sequences are widely adopted in musculoskeletal imaging protocols, in order to accurately display and evaluate cartilage, and in neuroimaging, even though their usage might be superseded by more accurate FLAIR sequences.

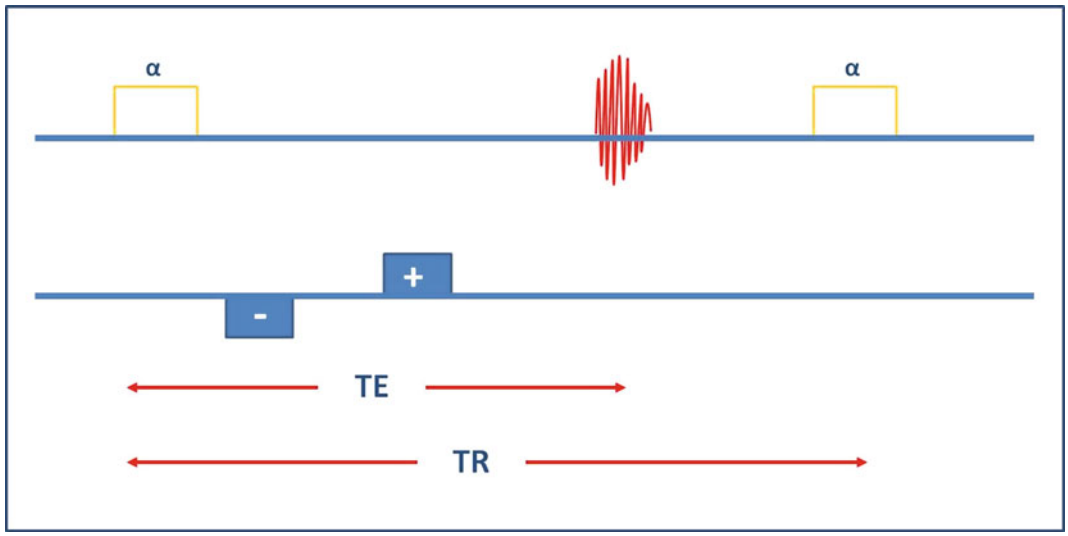

Fig. 9 Schematic representation of GE sequences. α slice-selective gradients are employed with limited flip angles (about 45°), dephasing and rephrasing of transverse magnetization are determined by alternated negative phase-encoding and positive frequency-encoding (readout) gradients

Table 1 Comparison between SE and GRE sequences

Comparison between SE and GRE sequences		
Parameter	SE	GRE
Rephasing system	RF pulse	Gradient variation
Flip angle	90° only	Variable
Efficiency at reducing magnetic inhomogeneity	Very efficient (true T2 effect)	Not very efficient (T2* weighted)
Acquisition time	Slow imaging	Fast imaging

2.2.5 Echo-Planar Imaging

This technique allows a significant shortening in acquisition time, since a single echo train is employed to acquire the entire volume. Echo-planar imaging (EPI) is available for both SE and GRE sequences; multiple lines of imaging data are acquired after a single RF excitation (single-shot EPI) or more RF pulses (multi-shot EPI). The latter guarantees higher spatial resolution and reduction of image distortion and signal loss due to susceptibility differences, T2 relaxation, and main field inhomogeneities [10]. Echo planar imaging is now a technique of choice for diffusion-weighted imaging (Fig. 16).

2.3 Dynamic Contrast-Enhanced MRI

Conventional static or phasic contrast-enhanced MRI is able to determinate vascularization of tissues, but gives no quantitative insight into hemodynamic processes, thus many dynamic contrast-enhanced (DCE) techniques have been designed, in order to provide further help in differential diagnoses of pathologic processes. The principal perfusional imaging technique is based on gadolinium bolus injection and subsequent acquisition of T1-weighted gradient echo sequence with short TE (<1.5 ms) and TR (<7 ms) and flip angle around 30° [11]. Due to high time resolution, these sequences permit to

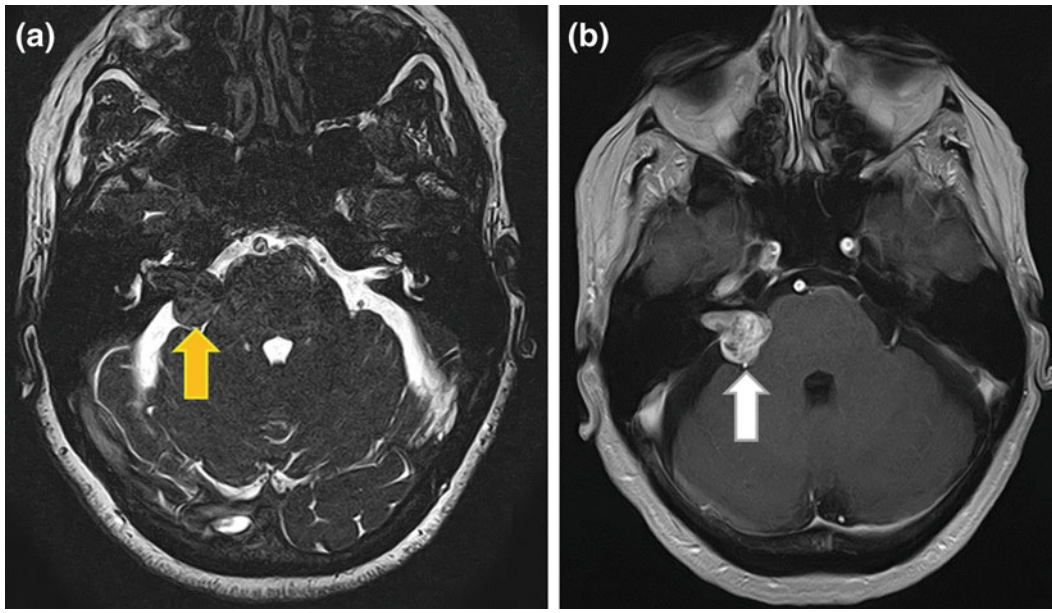

Fig. 10 Acoustic neuroma. This lesion classically present on imaging as a solid nodular mass with an intracanalicular component that often result in widening of the porus acusticus, as well demonstrated on CISS (constructive interference in steady state; *yellow arrow*) sequence (**a**) and confirmed on T1 post-Gd sequence (*white arrow*) (**b**)

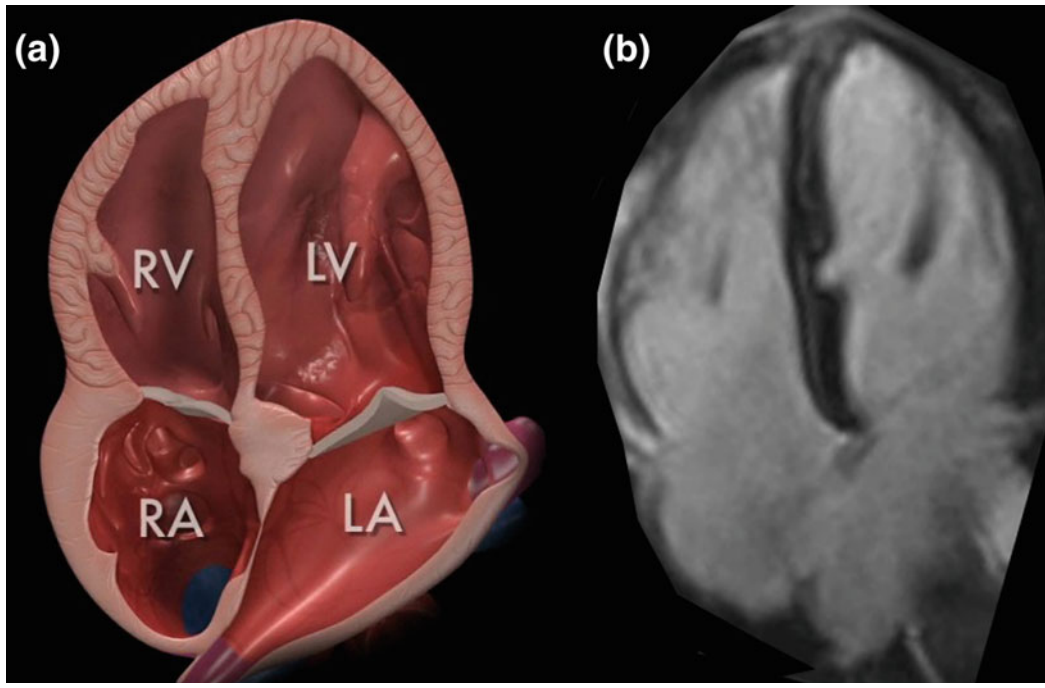

Fig. 11 Steady-state free precession (SSFP) imaging in cardiac MR. **a** 4 chambers plan of heart schematized. *RA* Right atrium. *LA* Left atrium. *RV* Right ventricle. *LV* Left ventricle. **b** 4 chambers SSFP imaging in patient with moderate right ventricular volume overload

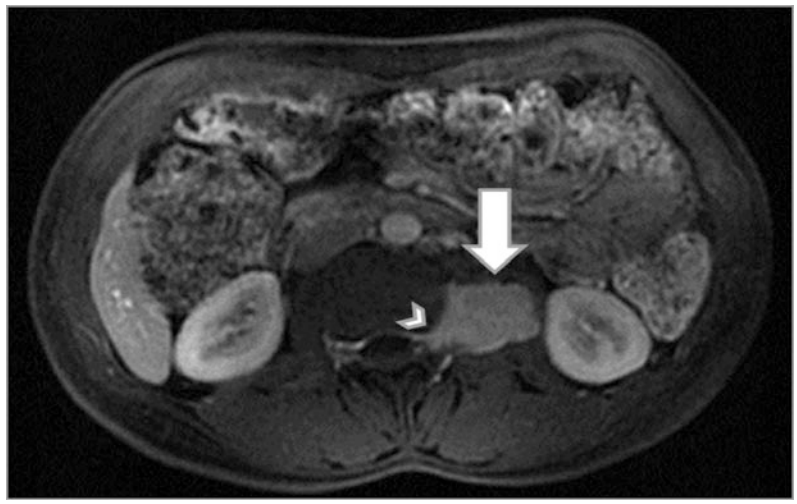

Fig. 12 T1-weighted fat-suppressed axial image, acquired after administration of Gadolinium, in a patient with left lumbar pain and paraesthesia. The study revealed a bulky left paravertebral mass with diffuse vascularization (*white arrow*) and 'dumbbell sign,' expression of relationship with the spinal cord. The final diagnosis was spinal schwannoma

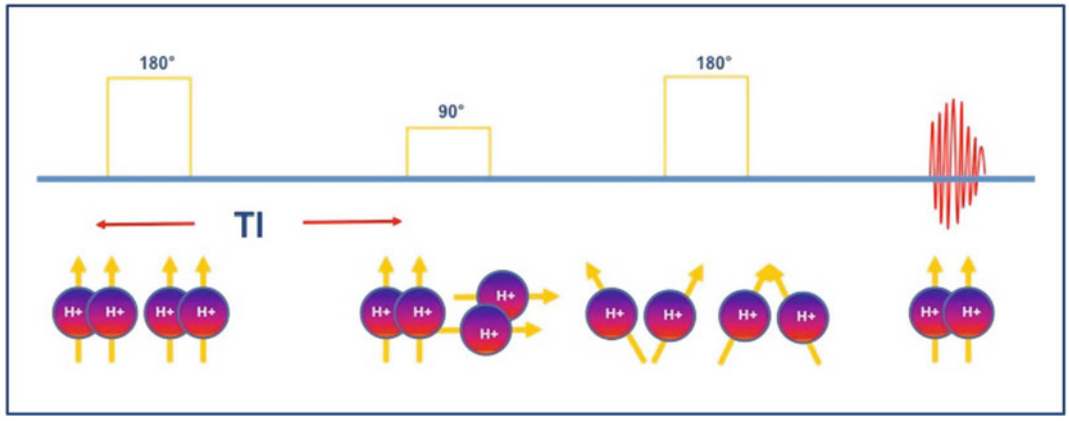

Fig. 13 Schematic representation of IR sequences. A 180° nulling RP is employed to suppress fat or water signal. After a determined inversion time (TI), a 90° pulse is applied to start the usual SE

acquire post-contrast consecutive images at several time points, in order to quantitatively evaluate contrast medium extraction. Through pharmacokinetic modeling of DCE data, a number of parameters can be determined, such as transfer constant (Ktrans) and fractional volume of the interstitial space (ve), deriving from these color map to display perfusion and permeability characteristics of tissues. The K-trans assessed in the first pass of contrast medium depicts cases where there is high permeability, while that measured in the steady state may better

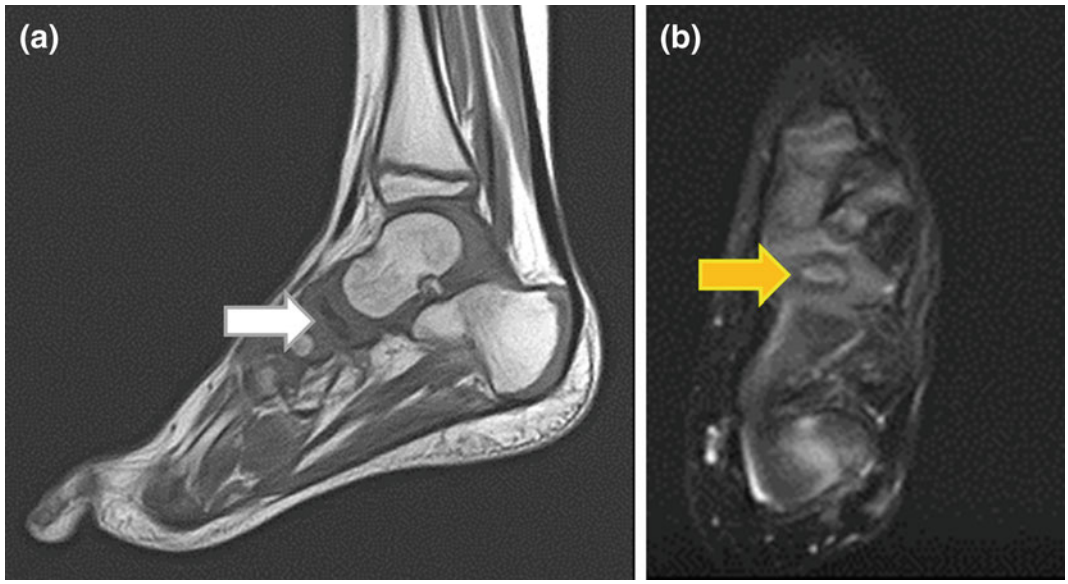

Fig. 14 Kohler's disease. Avascular necrosis of the navicular bone, detectable as an hypointensity on T1-w sequence (**a**, *white arrow*) and corresponding hyperintensity on STIR sequence (**b**, *yellow arrow*)

characterize situations of lower permeability, when Ktrans is dependent on surface area and is not flow limited (Fig. 17).

Many studies have addressed DCE-MRI to detection and characterization of neoplasms in many districts [12, 13], with great regard to CNS malignancy [14] (Fig. 18).

2.4 Magnetic Resonance Angiography (MRA)

Magnetic resonance angiography (MRA) has become an established imaging modality in management of vascular pathologies, from atherosclerotic condition (peripheral or carotid districts among the others) to vasculitis [15, 16]. MR Angiographic study can be performed with sequences with or without contrast medium. Both time-of-flight (TOF) and phase-contrast (PC) MRA are non-contrast techniques with intravascular blood detected by virtue of its movement compared with static surrounding tissues. Contrast-enhanced (CE) MRA relies on the T1 shortening effect of intravenously administered contrast media circulating in the blood. In TOF-MRA, vessel-to-background contrast is generated by the inflow of fresh, unsaturated blood in a saturated tissue slice [17]. Saturation of stationary background tissue is achieved by submitting it to radiofrequency pulses with a repetition time much shorter than tissue T1 values, thereby decreasing its longitudinal magnetization vector [18]. Because inflowing unsaturated blood still has a large longitudinal magnetization vector, it will be seen in the imaged slice as an area of high signal intensity. Intravascular protons are also subject to these saturation effects, which are proportional to the time protons reside in the imaging slice. Therefore short TR, slow flow, and course of the blood vessel in the imaging slice plane all unfavorably affect vessel-to-background contrast. TOF-MRA is possible by imaging successive, independent slices (2D TOF-MRA) or by imaging a volume that is later partitioned into separate slices (3D TOF-MRA). Although TOF-MRA is an attractive and entirely noninvasive method for imaging arteries, it is not widely applied because it suffers from a number of serious drawbacks. Currently, the main application of this sequence (particularly using 3D TOF MRA) regards the

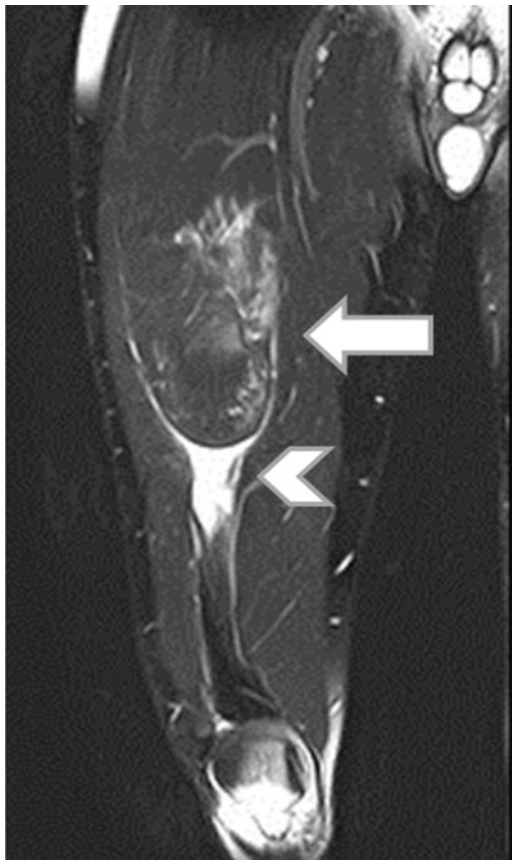

Fig. 15 Coronal T2-weighted STIR image in a young football player with severe right leg pain after accidental injury. Image shows diffuse oedema of the quadriceps (*white arrow*) and myotendinous junction complete tear with tendon retraction (*white arrowhead*)

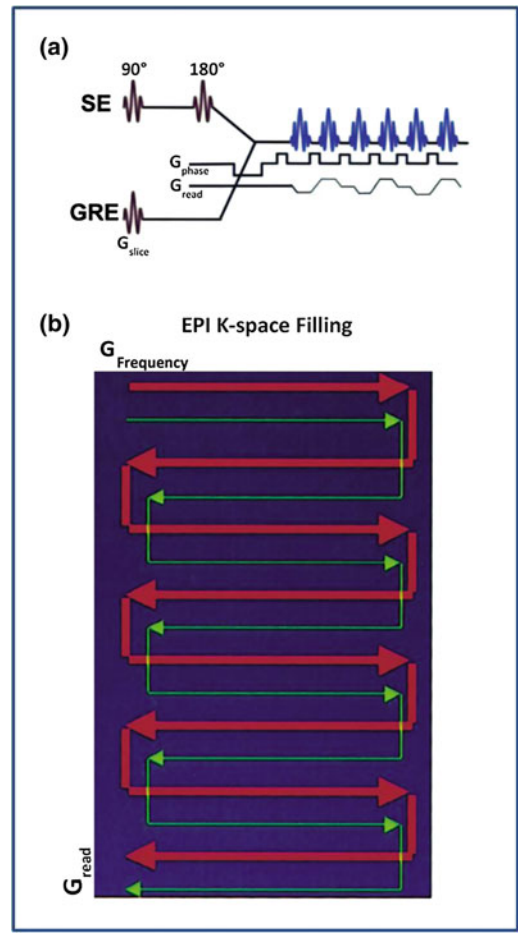

Fig. 16 **a** Schematic representation of echo-planar imaging for both SE and GRE techniques, with phase-encoding and frequency-encoding (readout) gradients rapidly turned on and off to shorten acquisition time. **b** K-space filling geometry in EPI

study of arterial circulation; in this context, TOF technique allows visualization of major intracranial arteries and peripheral branches in a relatively short time and generally does not require use of contrast agent, allowing a diagnostic depicting of pathological condition, sometimes associated with pain sensation, such as intracranial aneurysm (Fig. 19).

The clinical utility of TOF-MRA in other anatomical districts is limited by the long duration of image acquisition, a tendency for stenosis overestimation and different type of artifacts (motion artifacts, ghosting, flow void), but it can be useful as a backup modality in patients who cannot receive contrast medium.

Phase-contrast (PC)-MRA was developed as an alternative to TOF-MRA and uses an entirely different technique to generate vascular contrast. In PC-MRA, vessel-to-background contrast is generated by displaying the accumulated phase difference in transverse magnetization between moving protons in blood and stationary background tissues. PC MRA is based on the accumulated phase difference between mobile spins and stationary spins [19]. This characteristic renders PC acquisition more sensitive to slow flow, such as occurs in veins.

The introduction of MRI systems with higher gradients and fast breath-hold 3D sequences was

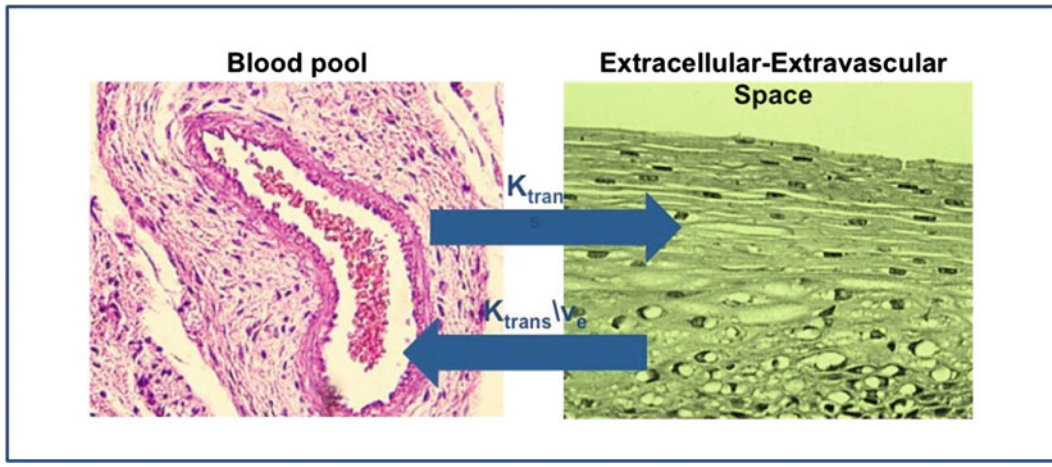

Fig. 17 Pharmacokinetic bicompartimental model on the basis of dynamic contrast-enhanced MRI. Ktrans is the tissue-specific constant that regulates contrast medium transfer to tumoral tissue. Ve expresses the percentage of tumoral tissue occupied by extracellular\extravascular space (interstitium)

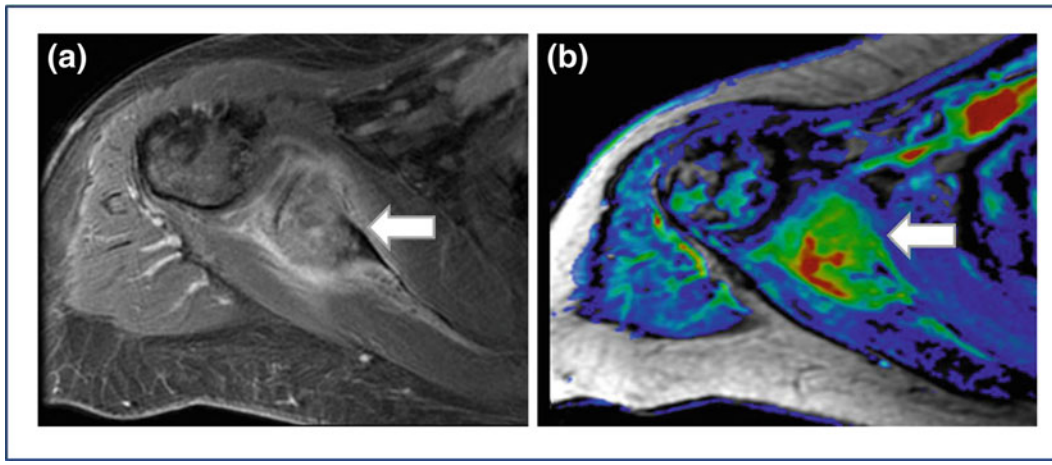

Fig. 18 **a** T1-weighted GRE fat-suppressed, dynamic contrast-enhanced, axial image of a painful metastatic lesion on right scapula. **b** Color map expressing Ktrans function for the same lesion, assessing a quantitative perfusional study

prerequisite for contrast-enhanced MR Angiography (CE-MRA). CE-MRA has improved spatial resolution compared with TOF, and PC-MRA and has helped to partially eliminate physiologic effects, such as turbulence leading to signal loss. This technique exploits the difference in the T1 relaxation times of blood and surrounding tissues when a rapid bolus infusion of a paramagnetic contrast agent is injected. These gadolinium-based agents exert a T1 shortening effect, generating a high intravascular SNR, which is largely unaffected by inflow. CE-MRA essentially needs a compromise between the desire for high spatial resolution and volumetric coverage (i.e., long acquisition duration), the desire to avoid disturbing venous enhancement (i.e., short acquisition duration), and high vessel-to-background contrast [20]. Rapid scan times are achievable by the use of fast-gradient sequences employing short TR. CE-MRA

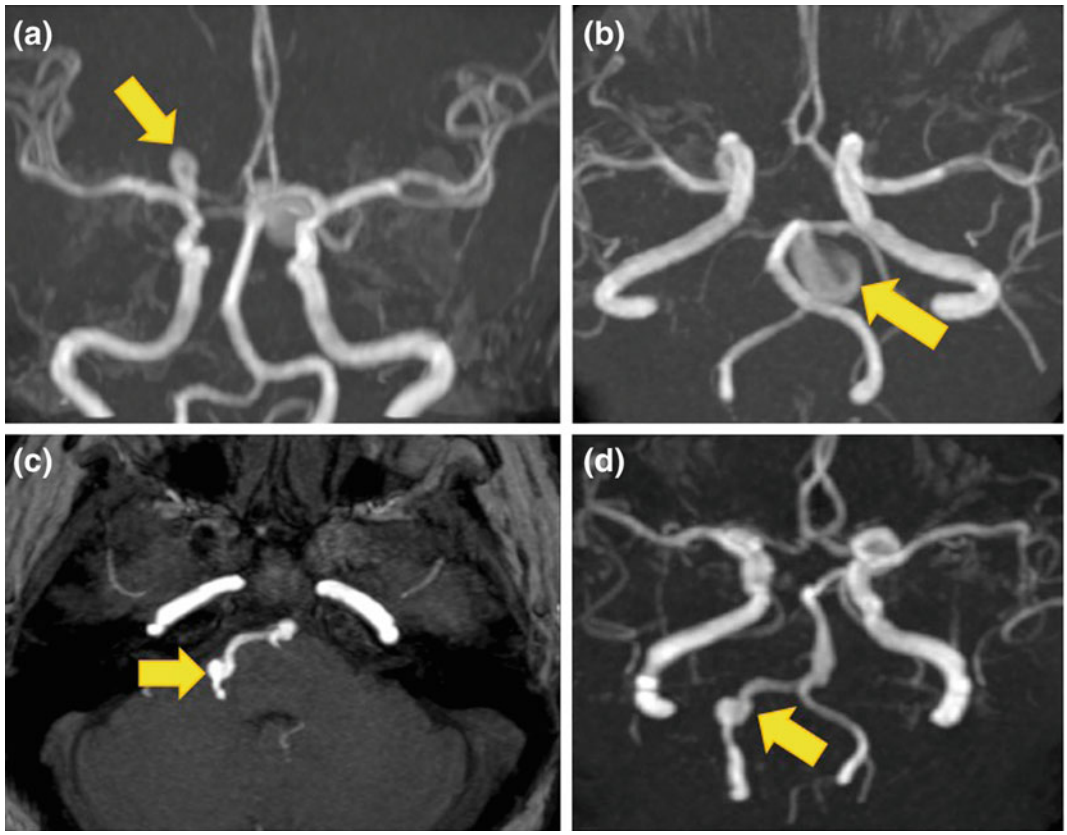

Fig. 19 Time-of-flight imaging of intracranial aneurysms in several localizations: right middle cerebral artery (**a**), basilar artery, ruptured (**b**) and right vertebral artery, at pontine level (**c**, **d**)

images are essentially a record of the vessel lumen, and timing of the scan is crucial to ensure high-quality images and avoid venous contamination. Because the time of peak arterial enhancement can vary substantially between patients, the CE-MRA examination must be tailored to the individual contrast arrival time. To determine the delay between the start of injection of contrast medium and the acquisition of central k-space profiles a 2D time-resolved test bolus technique can be used. However, more recently, bolus tracking techniques have been introduced to detect the arrival of contrast [21]; in contrast to injecting a small amount of contrast material in a separate test bolus scan, real-time bolus monitoring allows the operator to inject the total volume of contrast material, and to proceed with the 3D CE-MRA acquisition precisely when the desired signal enhancement in the arterial bed of interest has been detected by the scanner, or by visual feedback [22]. A following practical aspect of CE-MRA to consider is the vessel-to-background contrast. The T1 decrease into vessel, due to contrast medium injection, is not sufficient to selectively enhance arteries and to suppress background tissue; as a result, the signal of these tissues—and specifically, fat tissue—must be eliminated to present easily understandable images. The most commonly technique to do it is subtraction of non-enhanced 'mask' images, identical to the 3D CE-MRA volumes. Another important practical aspect to evaluate is venous enhancement and strategies to reduce this potential problem; this drawback is particularly prevalent in patients with cellulitis and AV malformations. There are different strategies to decrease the chance for disturbing venous enhancement, such as: increasing

acquisition speed, separate acquisition for the lower leg station, specialized k-space filling algorithms, time-resolved acquisition strategy, infrasystolic venous compression. The most straightforward way of preventing venous enhancement is by shortening acquisition duration. This should be done, first of all, by lowering TR and TE to the shortest possible value. An important technical evolution was achieved with development of dedicated centric k-space filling algorithms; this is useful for CE-MRA because the time between arterial and venous opacification is usually shorter than the duration of a high spatial resolution 3D CE-MRA acquisition. The underlying principle is to collect central k-space profiles, which primarily determine image contrast, at peak contrast enhancement in the arteries of interest whereas veins are not or only minimally enhanced. When peripheral k-space profiles are read out, primarily information encoding details in the image is acquired. When centric k-space filling is combined with parallel imaging, the chances of venous enhancement decrease even further [23].

All these improvements make this technique an important diagnostic tool in management of patients with vasculature symptoms, with the aim to recognize or characterize pathological findings responsible for painful condition (Fig. 20).

More sophisticated techniques use repetitive centric k-space filling to obtain high spatial resolution MR angiograms with high temporal frame rate. Korosec et al. were first to describe this concept, which they named Time-Resolved Imaging of Contrast Kinetics (TRICKS). With TRICKS the contrast-sensitive central part of k-space is sampled more often than the peripheral resolution-sensitive views [24]. After the acquisition is finished, central k-space lines are combined with peripheral lines through a process of temporal interpolation such that a series of time-resolved 3D images of the vasculature are obtained.

2.5 Diffusion-Weighted Imaging

Molecular diffusion, or Brownian motion, refers to the notion that any type of molecule in a fluid (e.g., water) is randomly displaced as the molecule is agitated by thermal energy. Diffusion-Weighted imaging (DWI) is a relatively new imaging technique that probes differences in Brownian motion of water molecules between tissues, reflecting histological organization [25].

Diffusion weighting enables to distinguish between rapid diffusion of protons (unrestricted diffusion) and slow diffusion of protons (restricted diffusion). For diffusion-weighted imaging, either an echo-planar or a fast GRE sequence is used. DWI is inherently a low-resolution and low-SNR technique and its low quality issues are also exacerbated by its high sensitivity to physiological motion. To reduce motion sensitivity, single-shot echo-planar imaging (EPI) is commonly used. The simplest configuration of this pulse sequence uses a pair of large gradient pulses placed on both sides of the 180° refocusing pulse. The first gradient pulse dephases the magnetization across the sample (or voxel in imaging); and the second pulse rephases the magnetization. For stationary (non-diffusing) molecules, the phases induced by both gradient pulses will completely cancel, the magnetization will be maximally coherent, and there will be no signal attenuation from diffusion. In other words, if no net movement of spinning nuclei occurs between the applications of the gradient pulses, the first gradient dephases the spins and the second rephases them; therefore, high signal intensity is seen. If there is net movement, the protons are not affected by both gradients (they may undergo dephasing but not rephasing, or vice versa); therefore, the signal intensity is decreased. The amount of signal loss is directly proportional to the degree of water motion. Signal loss is proportional to the motion component in the same direction as the diffusion gradient, while no signal loss would occur if the motion was perpendicular to the gradient direction.

The gradient strength, or more often the diffusion weighting, may be expressed in terms of the *b*-value. The *b*-value is proportional to the product of the diffusion time interval and the square of the strength of the diffusion gradient. A larger *b*-value is achieved by increasing the gradient amplitude

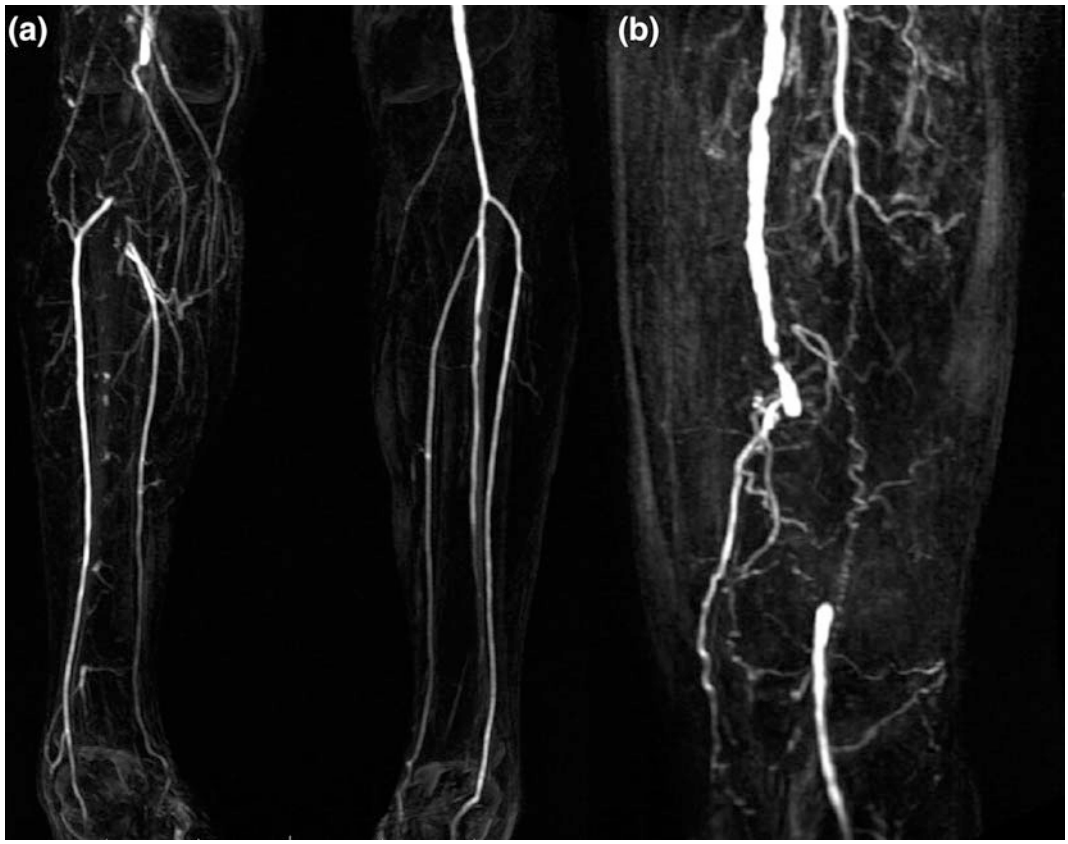

Fig. 20 Right popliteal artery occlusion in a patient with lower limb claudication. **a** Sagittal T1-weighted CE-MRA. **b** MIP reconstruction particular on right popliteal artery showing a chronic occlusion with collateral vessels development

and duration and by widening the interval between paired gradient pulses. To sense slow moving water molecules and smaller diffusion distances, *b*-value should be higher (e.g., $b = 550$ s/mm^2). All diffusion images should be compared with a reference image that is not diffusion weighted (a standard SE image), in which the strength of the diffusion gradient is zero.

The sensitivity of DWI to diffusion (characterized by its *b*-value) can be modified by altering the combination of gradient pulse amplitude, the time for which the gradients are applied and the time that elapses between their application. DWI has actually an important clinical application, however, imaging interpretation is not intuitive. To resolve this problem, let us assume that the diffusion has no restrictions and that its displacement distribution therefore can be described with a free diffusion physical model, which is a 3D isotropic Gaussian distribution. In this model, the physical diffusion coefficient D is replaced by the ADC, which is derived from the equation AD: $-b$ ln(DWI/b0), where DWI is the diffusion-weighted image intensity for a specific *b*-value and diffusion gradient direction, defined as in the previous section, and b0 is a reference image without diffusion weighting. In order to obtain an image of the ADC values, two acquisitions are necessary: one set obtained without application of a diffusion gradient (which have an appearance similar to that of T2-weighted images), and one obtained with a diffusion gradient. The ADC calculation is based on the negative logarithm of the ratio of those two image sets (images obtained with diffusion weighting compared with those obtained without

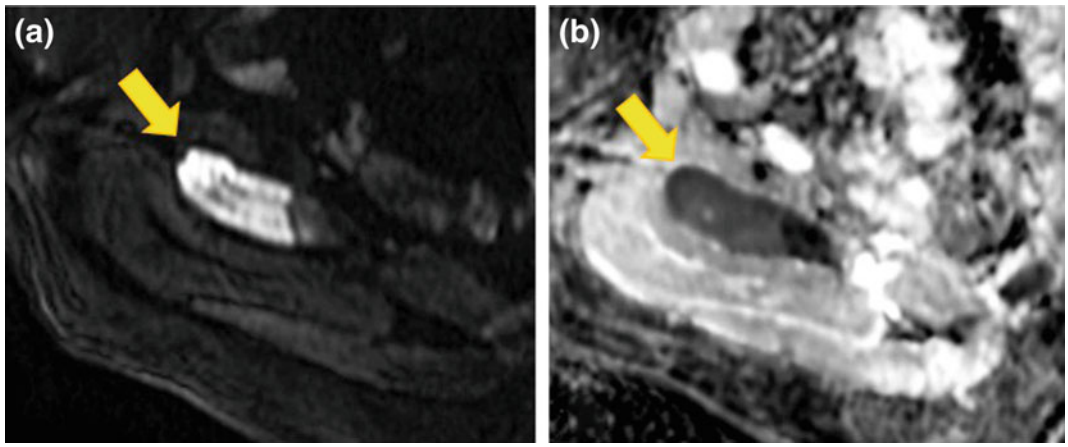

Fig. 21 **a** Painful right iliac bone metastasis with evidence of water diffusion restriction at DWI imaging (b = 1000 s \mm^2). **b** ADC map hypointensity confirms DWI detection

diffusion weighting). Even if stringent measures have been taken to avoid the effects of gross motion and flow, a diffusion-weighted image is still affected by MR properties other than that of diffusion, e.g., T2 weighting. To remove all effects other than that of diffusion, it is mandatory to use the apparent diffusion coefficient, as described. However, an ADC map created in this way by combining two images, with and without diffusion weighting or using two b-values, the lower of which is not large enough to remove the effects of perfusion, contains information about perfusion as well as diffusion components. To differentiate between perfusion and diffusion multiple b-values are needed.

The visualization of changes in the diffusion properties of tissue water with MR imaging has become a useful, multifaceted tool to characterize tissue structure and to identify and differentiate disease processes. DWI is routinely used in investigations of stroke in brain imaging [26]; it actually has a relatively new role in oncologic imaging, in which this technique has became an important tool used to characterize tumor cellularity. However, sometimes the appearance of high signal intensity on diffusion-weighted images also may be due to T2 effects, or so-called T2 shine-through. In clinical neurological practice, the absence of corresponding effects on ADC maps allows areas of restricted diffusion from recent stroke to appear dark and areas of unrestricted diffusion from older stroke to appear relatively bright. Therefore, DWI has always to be evaluated in comparison with ADC maps, in order to allow the determination of the age of a stroke (this concept should be always keep in mind during DWI evaluation in every clinical application). In oncologic management, DWI can use as a detection technique, able to identify some lesions (often causing unjustified pain, as in case of bone metastases), difficulty assessable with classic technique [27] (Fig. 21).

2.6 Diffusion Tensor Imaging

Diffusion tensor imaging (DTI) is an extension of DWI that allows data profiling based upon white matter tract orientation. In white matter (WM), diffusion follows the 'pathway of least resistance' along the WM tract; this direction of maximum diffusivity along the WM fibers is projected into the final image.

DTI is defined as a MRI technique that uses anisotropic diffusion to estimate the axonal—WM—organization of the brain, while fiber tractography (FT) is a 3D reconstruction technique to access neural tracts using data collected by DTI. In DTI, the anisotropy is utilized in order to estimate the axonal organization of the brain;

in fact, diffusion is anisotropic (directionally dependent) in WM fiber tracts, as axonal membranes and myelin sheaths present barriers to the motion of water molecules in directions not parallel to their own orientation. The direction of maximum diffusivity has been shown to coincide with the WM fiber tract orientation. This information is contained in the diffusion tensor, a mathematic model of diffusion in three-dimensional space [28]. The diffusion tensor describes the magnitude, the degree of anisotropy, and the orientation of diffusion anisotropy. By applying the appropriate magnetic field gradients, MR imaging may be sensitized to the random, thermally driven motion (diffusion) of water molecules in the direction of the field gradient. Since water tends to spread in the fibrous tissues (mainly in the WM) following the fiber orientation, diffusion tensor becomes an indicator of cognitive functional organization, allowing the identification of mutual connections between different functional centers and highlighting any possible alterations due to pathological situations [29]. Technically, tensor is a term used to describe a matrix of numbers derived from diffusion measurements in several different directions, from which it is possible to estimate the diffusivity in any arbitrary direction or determine the direction of maximum diffusivity [30]. The tensor matrix may be easily visualized as an ellipsoid whose diameter in any direction estimates the diffusivity in that direction and whose major principle axis is oriented in the direction of maximum diffusivity. The tensor model consists in a 3×3 matrix derived from the measurement of diffusivity in at least six noncollinear directions. At least six diffusion gradients and the corresponding ADC maps along six orthogonal directions (three orthogonal pure: *x*, *y*, *z*, and three combined: *xy*, *xz*, *yz*) in order to calculate the diffusion tensor. Using more than six encoding directions will improve the accuracy of the tensor measurement for any arbitrary orientation [31].

From a technical point of view, there are some considerations to make when assessing a diffusion tensor protocol. The protocol choice is moderately complicated by the wide spectrum of pulse sequence parameters that must be configured. The majority of DTI studies nowadays use *b*-values in the range of 700–1300 s/mm^2 (with a *b*-value of 1000 s/mm^2 being most common), leading to 30–50% signal reduction assuming the mean diffusivity of normal white matter is around $0.8–1.0 \times 10 - 3$ mm^2/s [32]. The determination of the optimum *b*-value is complicated by the involvement of many factors, including: SNR (the higher the SNR, the more accurately signal attenuation can be measured with higher *b*-values), echo time (the smaller the *b*-value, the shorter the achievable echo time), and other factors that are more difficult to assess such as eddy current and motion artifacts (in general, smaller *b*-values produce less artifacts). Measurements of diffusion anisotropy tend to be quite sensitive to image noise, which can also lead to biases in the anisotropy estimates [33]. The accuracy of DTI measures may be improved by either increasing the number of encoding directions or increasing the number of averages. Unfortunately, this increases the scan time for DTI data collection [34].

The information contained in the diffusion tensor can be "viewed" through creation of maps of appropriate diffusion indices derived from DTI data, of which the main are represent by mean diffusivity (MD) or in other term apparent diffusion coefficient (ADC), and fractional anisotropy (FA). Specifically, MD reflects the average magnitude of molecular displacement by diffusion (the more the MD value, the more the isotropic is the medium), while FA reflects the directionality of molecular displacement by diffusion and vary between 0 (isotropic diffusion, such as in CSF) and 1 (infinite anisotropic diffusion). In particular, the FA provides information regarding to the shape of rotation ellipsoid associated with the tensor: starting from the null value for FA is the shape is spherical (isotropic diffusion); higher values of FA correspond to shapes ellipsoid more elongated, up to reach the linear form for FA = 1 (maximum anisotropy).

Another important measure is the tensor orientation described by the major eigenvector direction. For diffusion tensors with high anisotropy, the major eigenvector direction is

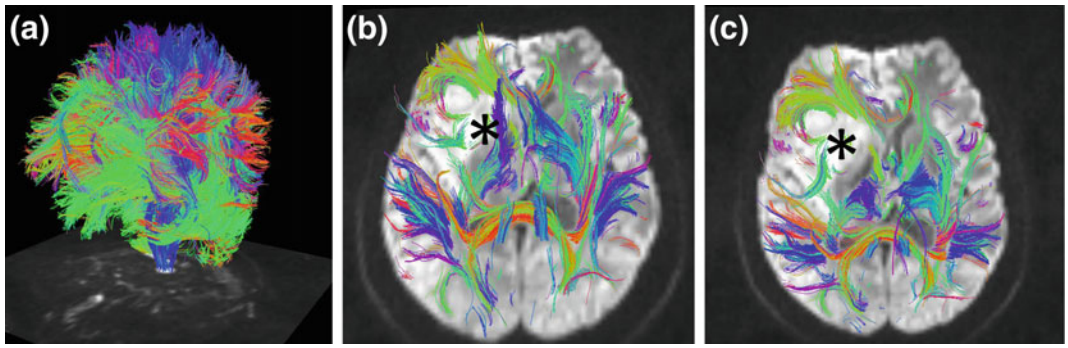

Fig. 22 **a** Full brain volume fiber tracking from DTI datasets in a patients with right frontal lobe glioma. Axial–oblique view (**b**) and axial view (**c**), with thin slice segmentation, demonstrating the fibers around the tumor (*asterisks*)

generally assumed to be parallel to the direction of white matter tract, which is often represented using an RGB (red-green-blue) color map to indicate the eigenvector orientations. The local eigenvector orientations can be used to identify and parcellate-specific WM tracts; thus DT-MRI has an excellent potential for applications that require high anatomical specificity. This technique, preparatory to the implementation of tractography, represents excellent ability of this technique in anatomic functional WM depiction make it an important and innovative tool in pre- and postoperative management of patient with brain lesions [35].

DTI has been reported in a broad spectrum of applications, such as in assessment of WM deformation determined by tumors, in pre-surgical planning (Fig. 22), in Alzheimer disease (to detect an early phase of disease), in schizophrenia, in focal cortical dysplasia, and in multiple sclerosis (for plaque assessment).

The primary reason is that water diffusion in tissues is highly sensitive to differences in the microstructural architecture of cellular membranes. Increases in the average spacing between membrane layers will increase the apparent diffusivity, whereas smaller spaces will lead to lower apparent diffusivities. This sensitivity makes DTI a powerful method for detecting microscopic differences in tissue properties. However, the interpretation of changes in the measured diffusion tensor is complex and should be performed with care; in particular, FA is highly sensitive to microstructural changes, but not very specific to the type of changes.

2.7 MR Spectroscopy

Magnetic resonance spectroscopy (MRS) is an imaging technique able to depict neurochemical function of a volume-of-interest (VOI) [36]. MRS technique has been initially developed to determinate chemical and biochemical properties of some compounds in solution; the introduction of gradient field technology in MRI permitted the evolution of in vivo spectroscopy. Biological and medical spectroscopy applications are mainly addressed to ^{1}H, ^{13}C, 19F, and ^{31}P isotopes. MRS technique requires high-intensity static magnetic fields (at least 1.5 T) in order to ensure better homogeneity and increased sensitivity. In vivo MR spectroscopy is analyzed on the basis of three different parameters: chemical shifts, signal intensities, and spin–spin (J) coupling [37]. While chemical shifts and J-couplings provide qualitative information on the chemical structure, signal intensities provide information on different concentrations of compounds. The chemical shift is defined as the ratio of the resonance frequency difference between the signal of interest (n) and a reference signal ($n$ref) relative to the operating frequency of the MR system (n0), and is expressed in units of ppm. Chemical shifts are used to characterize in vivo different compounds, employing the property of local chemical

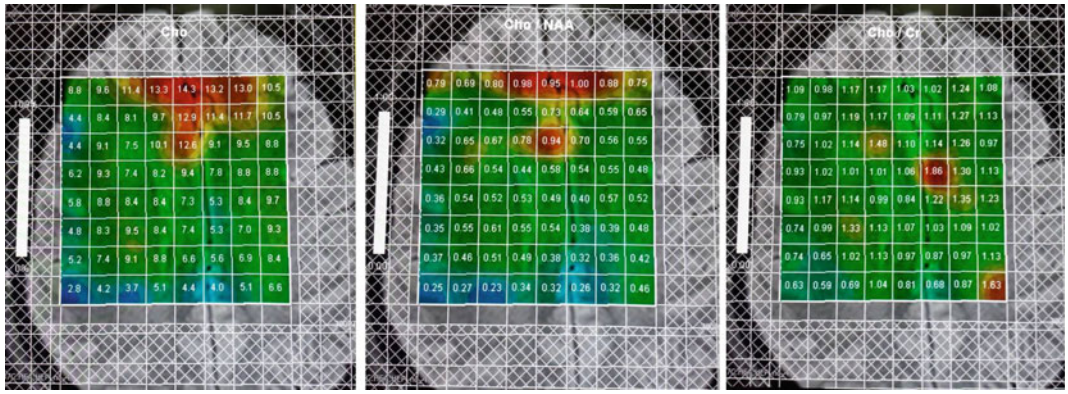

Fig. 23 Multiple voxel spectroscopy. *Panel* showing an assessment of different metabolites in patient with solid brain lesions

environment and molecular bonding to affect the distribution of electron density around a nucleus and to modify the resonance frequencies. Resonances of the methyl groups of N-acetylaspartate (NAA, d = 2.01 ppm) or creatine (Cr, d = 3.02 ppm) are typically used as internal chemical shift references for in vivo MRS applications. Resonance signals can be displayed as single peaks (singlets) or can be split into several signals (multiplets). MRS highlights the split resonances, caused by spin–spin coupling (J-coupling) between neighboring protons. The strength of coupling is defined by the J-coupling constant and can be extracted from the splitting pattern of the spectral multiplet. Intensities of resonance signals (measured as amplitudes or integrals of the areas under the signals) are proportional to the concentration and to the number of corresponding magnetically equivalent nuclei in a molecule.

2.7.1 MR Spectroscopic Imaging

MRS can be performed using different techniques. Opportune setting of TR and TE is crucial; in particular, some specific investigations require short echo times (TE = 20–35 ms) to detect metabolites with short relaxation times, such as glutamate, glutamine, myoinositol, glycine, GABA, and some amino acids. Cr is a relatively stable metabolite, requiring a long TE to be observed (100 ms or more); it is widely employed as internal control for deriving other metabolites concentrations. Single-voxel spectroscopy (SVS) is the most time-efficient modality, offering a spatial resolution in the order of 1–8 cm^3. It analyzes the signal from a given VOI of a tissue. Multiple voxel techniques, known as chemical shift imaging (CSI) or magnetic resonance spectroscopic imaging (MRSI), permit the derivation of metabolite maps (Fig. 23). The CSI is able to include larger volumes of tissue in the spectroscopy study with possible separate voxel-by-voxel analysis of the entire acquired volume. These voxels can be as small as 1 cm^3. MRS is hampered by several limitations, such as artifacts due to high differences in magnetic susceptibility (bone, air, large vessels, metals).

In the last years, several studies have expressed relationships between *N*-acetyl aspartate (NAA) and glucose metabolism in determinate brain areas (most importantly prefrontal cortex, anterior cingulate cortex and thalamus) and painful syndromes. Kupers and colleagues studied 13 healthy volunteers after painful heat stimulation to the right, revealing a GABA concentration increase of 15% in the rostral anterior cingulate cortex (rACC), by single-voxel ^{1}H-MRS at a 3T scanner with a short TE (20 ms) [38].

2.8 Susceptibility Weighted Imaging

This sequence is a high spatial resolution 3D gradient echo MR imaging technique with phase

post-processing that accentuates the paramagnetic properties of blood products and is very sensitive in the detection of intravascular venous deoxygenated blood as well as extravascular blood products [39]. Because of its ability in blood products detection, SWI is becoming a new exciting tool used in studies of arterial venous malformations, occult venous disease, multiple sclerosis, trauma, tumors and functional brain imaging [40]. SWI exploits the loss of signal intensity created by disturbance of a homogeneous magnetic field; various paramagnetic, ferromagnetic, or diamagnetic substances such as air/tissue or air/bone interfaces can be responsible of these disturbance. Sensitivity to susceptibility effects increase as one progresses from fast spin-echo to routine spin-echo to gradient echo techniques, from T1- to T2- to T2*-weighting, from short-to-long echo times, and from lower to higher field strengths. After data acquisition, additional post-processing can accentuate the signal intensity loss caused by any susceptibility effects. The phase images are high-pass filtered and then transformed to a special mask that varies in amplitude between zero and unit; this mask is multiplied a few times into the original magnitude image, in order to generate enhanced contrast between paramagnetic substances and surrounding tissue. Actually, SWI has as a main application the identification of small amounts of hemorrhage/blood product or calcium, booth possibly unapparent on other MRI sequences [41].

2.9 BOLD Functional MRI

The rationale of blood oxygenation level-dependent (BOLD) magnetic resonance imaging is that blood flow would sensitively depict the tissue's activity [42]. The BOLD contrast method employs the electromagnetic property of deoxygenated hemoglobin (dHb) to suppress fMRI signal generated from neighboring water molecules. The increase in level of oxygenation of the blood required by tissue's activity is displayed by BOLD imaging as a decrease in dHb suppression, and thus as an increase in fMRI signal. Disadvantages of BOLD fMRI mainly consist in the unfeasibility to assess a baseline fMRI signal, since BOLD signal measures change between alternating states, and in the weakness of fMRI signal compared to PET imaging. Venous BOLD functional imaging employs T2*-weighted sequences, particularly sensitive to magnetic field inhomogeneities, thus able to read out changes in dHb\water interaction both in intravascular and extravascular spaces [43]. BOLD imaging can be performed with both SE and GE techniques; the latter are mostly employed because of their relatively high sensitivity at the cost of limited spatial resolution. Another fMRI technique is quantitative assessment of blood volume to a determinate tissue by administration of iron oxide contrast agents. Using T2*-w sequences, an increase in blood volume to a tissue induces an increase in the content of contrast agents, and consequently a decrease in MRI signal. The use of noninvasive neuroimaging methods including BOLD fMRI has been utilized to clarify the neural bases of many kinds of sensorimotor and mental processes in neuroscience. fMRI has an extensive role in neuroimaging. Initial pain neuroimaging experiences have studied location and pattern of neural activity evoked by a painful or non-painful stimulus. These studies revealed a common whole brain activation pattern (comprehending primary and secondary somatosensory cortex, cerebellum, anterior insular and cingulate cortices, basal ganglia, and both frontal regions and posterior parietal cortex) responding to mechanical, heat, cold, and electrical stimuli, and unique stimuli, referred to as a network or the 'pain matrix' (Fig. 24).

2.10 MR Thermometry in Focused Ultrasound Ablative Technique

The development of MRI techniques able to noninvasively measure temperature changes in tissue led physicians to look at these with high interest to enhance the guidance of thermal

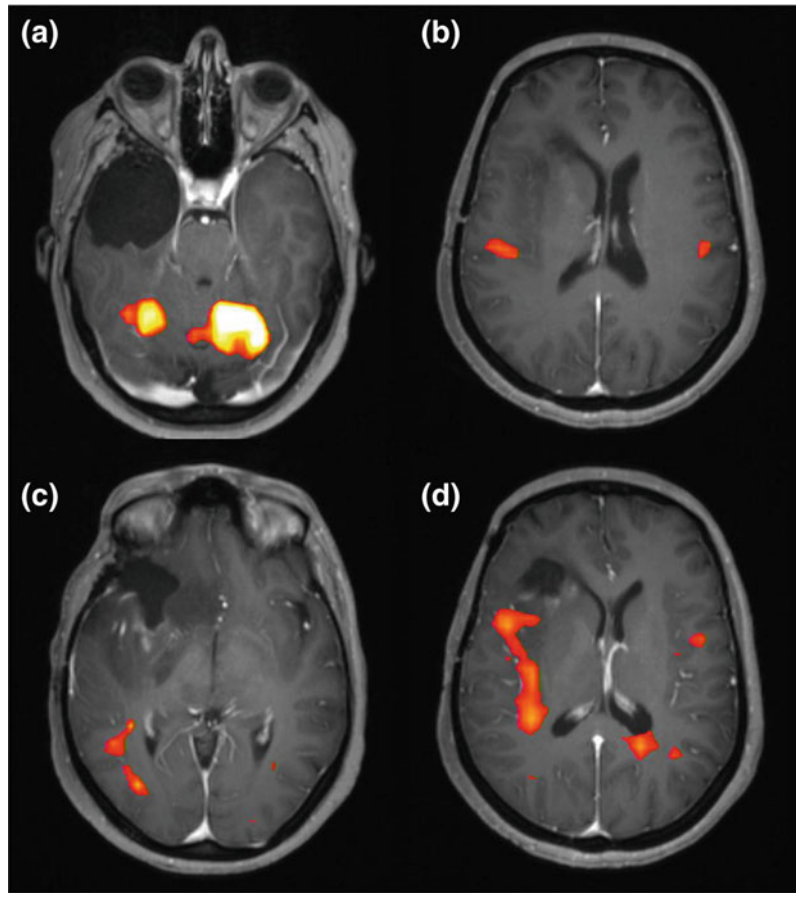

Fig. 24 Patient with recurrent cerebral tumor; pre-surgical evaluation with fMRI and BOLD sequences. Absence of close contiguity relations between the areas of activation (left hand **a**, **b** and left foot **c**, **d**) and recurrent lesion and the above described lesion known

therapy treatments (such as Magnetic Resonance guided Focused Ultrasound). A possible technique able to assess temperature tissue changes is diffusion weighted; molecular water mobility due to thermal Brownian motion is quantified by the molecular diffusion coefficient of water, which is, by definition, a temperature-dependent process and can be quantified using MRI via the apparent diffusion coefficient. By far, the most exploited and widely validated quantitative MRTI techniques are based on the temperature sensitivity of the water proton chemical shift [44]. The shift of the PRF is proportional to temperature over a large range of temperatures (0–100 °C), with a sensitivity of % 0.01 ppm/°C for bulk water. Similar to the previous method, the physical basis for the temperature-dependent PRF phenomenon is that a rise in temperature leads to a corresponding increase in molecular Brownian motion. The result of this is that, as temperature rises, hydrogen bonds between local water molecules bend, stretch, and break. Using MRI, this temperature-dependent PRF shift can be measured using chemical shift imaging (CSI) techniques to directly measure the frequency shift. However, the easiest method for fast, high-resolution estimation of temperature changes due to the PRF shift is based on indirect measurements via relating the difference in phase between subsequent images to the frequency shift. A shift in the PRF is linearly related to temperature and can be mapped rapidly with standard

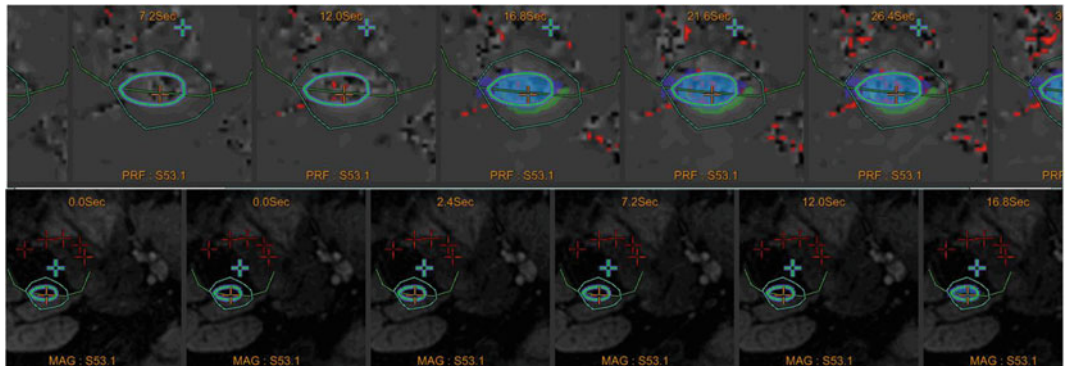

Fig. 25 MR thermography monitoring MRgFUS ablation by a real-time color map with blue area representing major heat

MR imaging sequences using phase differences. However, the conventional MR thermometry is insensitive to temperature changes in fat and is susceptible to motion artifacts including tissue swelling due to the need for image subtraction. The primary disadvantage of using standard CSI techniques is poor spatiotemporal resolution, limiting the ability to directly apply this technique for monitoring rapid heat delivery in a volume. In the clinical practice, an ablative non-invasive image-guided treatment (such as High-Intensity Focused Ultrasound, HIFU) may be improved by using of real-time thermal mapping with phase-difference fast-spoiled gradient-echo MR imaging, which is performed at the targeted region before, during, and immediately after sonication [45]. These images are automatically compared with a reference image obtained immediately before the sonications in order to generate a real-time thermal map (Fig. 25).

Thermal feedback is generated by real-time PRF while magnitude images highlight the temperature changes and the anatomy in the targeted area [46]. A temperature graph shows the temperature change on the temperature maps (Fig. 26).

The benefit of combining MR with the focused ultrasound treatment is real-time monitoring of the localization of the individual sonications, enabling the measurement of energy deposition and the temperature changes in the region being treated, and feedback on the effectiveness and safety of the sonications, allowing to obtain a quantitative real time image of an effect, with a comparative evaluation between temperature analysis, patient sensations, and sonication effects.

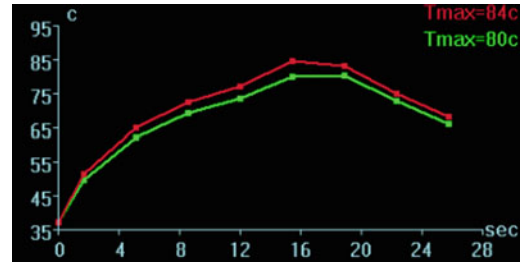

Fig. 26 Temperature versus time curve monitoring thermal energy administered by MrgFUS sonication

References

1. Merskey H, Bogduk N. Classification of chronic pain. IASP Task Force on Taxonomy. 2nd ed. Seattle: IASP Press; 1994.
2. Tracey I. Imaging pain. Br J Anaesth. 2008;101 (1):32–9.
3. Albe-Fessard D, Berkley KJ, Kruger L, Ralston HJ, III, Willis WD, Jr. Diencephalic mechanisms of pain sensation. Brain Res. 1985;356:217–96. Apkarian AV, Bushnell MC, Treede RD, Zubieta JK. Human brain mechanisms of pain perception and regulation in health and disease. Eur J Pain. 2005;9:463–84.
4. Harris RE, Sundgren PC, Pang Y, et al. Dynamic levels of glutamate within the insula are associated with improvements in multiple pain domains in fibromyalgia. Arthritis Rheum. 2008;58(3):903–7.
5. Khan HS, Stroman PW. Inter-individual differences in pain processing investigated by functional

magnetic resonance imaging of the brainstem and spinal cord. Neuroscience. 2015;29(307):231–41.
6. Jongen JL, Hans G, Benzon HT, et al. Neuropathic pain and pharmacological treatment. Pain Pract. 2014;14(3):283–95.
7. Narváez JA, Narváez J, De Lama E et al. MR imaging of early rheumatoid arthritis. Radiographics. 2010;30(1):143–63; discussion 163-5.
8. Brown MA, Semelka RC. MR imaging abbreviations, definitions, and descriptions: a review. Radiology. 1999;213:647–62.
9. McRobbie DW, Moore EA, Graves MJ et al. MRI from picture to proton. 2nd ed. 2010. Cambridge: Cambridge University Press.
10. Mirowitz SA, Brown JJ, McKinstry RC, Li Tao. Principles and applications of echo-planar imaging: a review for the general radiologist. Mehdi Poustchi-Amin. RadioGraphics. 2001;21(3):767–79.
11. Choyke PL, Dwyer AJ, Knopp MV. Functional tumor imaging with dynamic contrast-enhanced magnetic resonance imaging. J Magn Reson Imaging. 2003;17(5):509–20.
12. Bali MA, Metens T, Denolin V, et al. Tumoral and nontumoral pancreas: correlation between quantitative dynamic contrast-enhanced MR imaging and histopathologic parameters. Radiology. 2011;261 (2):456–66.
13. Bhooshan N, Giger ML, Jansen SA, et al. Cancerous breast lesions on dynamic contrast-enhanced mr images: computerized characterization for image-based prognostic markers. Radiology. 2010;254(3):680–90.
14. Lacerda S, Law M. Magnetic resonance perfusion and permeability imaging in brain tumors. Neuroimaging Clin N Am. 2009;19(4):527–57.
15. Meaney JF, Ridgway JP, Chakraverty S, et al. Stepping-table gadolinium-enhanced digital subtraction MR angiography of the aorta and lower extremity arteries: preliminary experience. Radiology. 1999;211:59–67.
16. Ho KY, Leiner T, de Haan MW, et al. Peripheral MR angiography. Eur Radiol. 1999;9:1765–74.
17. Shigematsu Y, Korogi Y, Hirai T, et al. 3D TOF turbo MR angiography for intracranial arteries: phantom and clinical studies. J Magn Reson Imaging. 1999;10:939–44.
18. Wedeen VJ, Meuli RA, Edelman RR, et al. Projective imaging of pulsatile flow with magnetic resonance. Science. 1985;230:946–8.
19. Walker MF, Souza SP, Domoulin CL. Quantitative flow measurement in phase contrast MR angiography. JCAT. 1988;12:304–13.
20. Hentsch A, Aschauer MA, Balzer JO et al. Gadobutrolenhanced moving-table magnetic resonance angiography in patients with peripheral vascular disease: a prospective, multicentre blinded comparison with digital subtraction angiography. Eur Radiol. 2003;13:2103–14.
21. Luccichenti G, Cademartiri F, Ugolotti U, et al. Magnetic resonance angiography with elliptical ordering and fluoroscopic triggering of the renal arteries. Radiol Med (Torino). 2003;105:42–7.
22. Wang Y, Chen CZ, Chabra SG, et al. Bolus arterial-venous transit in the lower extremity and venous contamination in bolus chase threedimensional magnetic resonance angiography. Invest Radiol. 2002;37:458–63.
23. Willinek WA, Gieseke J, Conrad R, et al. Randomly segmented central k-space ordering in high-spatial-resolution contrast-enhanced MR angiography of the supraaortic arteries: initial experience. Radiology. 2002;225:583–8.
24. Korosec FR, Frayne R, Grist TM, et al. Time-resolved contrast-enhanced 3D MR angiography. Magn Reson Med. 1996;36:345–51.
25. Mori S, Barker PB. Diffusion magnetic resonance imaging: its principle and applications. Anat Rec. 1999;257:102–9.
26. Roberts TP, Rowley HA. Diffusion weighted magnetic resonance imaging in stroke. Eur J Radiol. 2003;45:185–94.
27. Charles-Edwards EM, de Souza NM. Diffusion-weighted magnetic resonance imaging and its application to cancer. Cancer Imaging. 2006;6:135–43.
28. Mori S, Zhang J. Principles of diffusion tensor primer imaging and its applications to basic neuroscience research. Neuron. 2006;51:527–39.
29. Hagmann BP, Jonasson L, Maeder P, et al. Understanding diffusion MR imaging techniques: from scalar diffusion-weighted imaging to diffusion tensor imaging. RadioGraphics. 2006;26:S205–23.
30. Alexander AL, Lee JE, Lazar M, Field AS. Diffusion tensor imaging of the brain. Neurotherapeutics. 2007;4(3):316–29.
31. Basser PJ, Matiello J, Le Bihan D. MR diffusion tensor spectroscopy and imaging. Biophys J. 1994;66:259–67.
32. Tournier JD, Mori S, Leemans A. Diffusion tensor imaging and beyond. Magn Reson Med. 2011;65 (6):1532–56.
33. Pierpaoli C, Basser PJ. Toward a quantitative assessment of diffusion anisotropy. Magn Reson Med. 1996;36:893–906.
34. Moseley ME, Cohen Y, Kucharczyk J, et al. Diffusion-weighted MR imaging of anisotropic water diffusion in cat central nervous system. Radiology. 1990;176:439–46.
35. Pajevic S, Pierpaoli C. Color schemes to represent the orientation of anisotropic tissues from diffusion tensor data: Application to white matter fiber tract mapping in the human brain. Magn Reson Med. 1999;42:526–40.
36. Tran T, Ross B, Lin A. Magnetic resonance spectroscopy in neuro-logical diagnosis. Neurol Clin. 2009;27(1):21–60.
37. Grachev ID, Fredrickson BE, Apkarian AV. Abnormal brain chemistry in chronic back pain: an in vivo proton magnetic resonance spectroscopy study. Pain. 2000;89:7–18.

38. Kupers R, Danielsen ER, Kehlet H, Christensen R, Thomsen C. Painful tonic heat stimulation induces GABA accumulation in the prefrontal cortex in man. Pain. 2009;142:89–93.
39. Haacke EM, Xu Y, Cheng YC, et al. Susceptibility weighted imaging (SWI). Magn Reson Med. 2004;52:612–8.
40. Sehgal V, Delproposto Z, Haacke EM, et al. Clinical applications of neuroimaging with susceptibility-weighted imaging. J Magn Reson Imaging. 2005;22:439–50.
41. Pauling L, Coryell CD. The magnetic properties and structure of hemoglobin, oxyhemoglobin and carbonmonoxyhemoglobin. Proc Natl Acad Sci U S A. 1936;22:210–6.
42. Vincent K, Moore J, Kennedy S, Tracey I. Blood oxygenation level dependent functional magnetic resonance imaging: current and potential uses in obstetrics and gynaecology. BJOG. 2008;116 (2):240–6.
43. Price RR, Allison J, Massoth RJ et al. Practical aspects of functional MRI (NMR Task Group #8). Med Phys. 2002;29(8).
44. McDannold N. Quantitative MRI-based temperature mapping based on the proton resonant frequency shift: review of validation studies. Int J Hyperther. 2005;21(6):533–46. 27.
45. Graham SJ, Chen L, Leitch M, et al. Quantifying tissue damage due to focused ultrasound heating observed by MRI. Magn Reson Med. 1999;41:321–8.
46. Kuroda K, Oshio K, Chung AH, Hynynen K, Jolesz FA. Temperature mapping using the water proton chemical shift: a chemical shift selective phase mapping method. Magn Reson Med. 1997;38 (5):845–51.